



**Fermi National Accelerator Laboratory**

**FERMILAB-Conf-89/261-E**  
[E-741/CDF]

## **Jet Dynamics at the Tevatron Collider\***

The CDF Collaboration

*presented by*

Robert Plunkett  
*Fermi National Accelerator Laboratory*  
*P.O. Box 500*  
*Batavia, Illinois 60510*

December 1989

\* Published in the proceedings of the 8th Topical Workshop on  $p\bar{p}$  Collider Physics, Castiglione della Pescaia, Italy, September 1-5, 1989.



# JET DYNAMICS AT THE TEVATRON COLLIDER

CDF Collaboration\*

Presented by Robert Plunkett

Fermi National Accelerator Laboratory

P.O. Box 500

Batavia, IL 60510, USA

Results for processes involving two or more hadronic jets at  $\sqrt{s} = 1800$  GeV are presented. The data are compared with the results predicted from perturbative QCD.

## INTRODUCTION

This paper describes several measurements made by the CDF collaboration to test the range and scope of the validity of QCD, the widely accepted theory of the strong interaction of hadrons (by their constituent quarks and gluons). The tests all involve the dynamics of jet production in proton-antiproton collisions (at a CM energy of 1800 GeV); their unifying theme is perturbative QCD. The measurements to be described may be conveniently grouped into two principal categories:

- 1) Measurements involving the kinematical relationships among jets in events, and
- 2) Measurements inside a given jet (fragmentation studies and production of exclusive channels).

Of these two categories, the first is clearly more inclusive than the second. Inside each category as well, we will group our measurements by degree of exclusivity, which is correlated with the number of kinematic variables required to describe the process. Thus in the first category we will begin with the measurement of the double differential cross section for events with at two or more jets, where one jet is constrained to be at a rapidity of nearly zero (central in the CDF detector). The relevant kinematical variables in this case are  $y_2$  (the rapidity of the next-to-leading jet), and  $P_t$  (the momentum transverse to the beamline of the final state parton). We then proceed to discuss three-jet events, described by five kinematical variables.

The second category consists of measurements of the properties of individual particles inside jets. Our first measurement is of the charged fragmentation function  $D(Z)$ , which gives the probability that a

---

\* CDF collaborating institutions are listed in the Appendix.

charged particle will carry a given fraction  $Z$  of the jet momentum. This function is expected to show characteristic violations of scaling if QCD bremsstrahlung is occurring during the evolution of the jet. Lastly we consider the production of specific flavors of quarks inside a QCD jet, in this case the  $c$  quark as tagged by the production of  $D^*$ 's.

All of these measurements must be evaluated in the context of considerable systematic errors on both the measurement itself (usually dominated by the jet energy scale) and on the theoretical predictions of perturbative QCD (usually due to lack of detailed information on higher-order corrections, leading, e.g., to significant dependencies on choice of renormalization scale). This is typical of the situation today in tests of QCD. Nevertheless, the information we present favors the predictions of perturbative QCD over a wide range of process types, energy scales, and angular distributions.

## STUDIES OF JET KINEMATICAL DISTRIBUTIONS

### Two Jet Differential Cross Section -- 1987 Data

The process  $\bar{p}p \rightarrow \text{jet1} + \text{jet2} + X$  may be described by the differential cross section  $\frac{d^3\sigma}{dE_t d\eta_1 d\eta_2}$ , where  $\eta_1$  and  $\eta_2$  are the pseudo-rapidities of the two leading jets and  $E_t$  is the transverse energy of the leading jet. We use the variables  $\eta_1$ ,  $\eta_2$ , and  $E_t$  instead of the related set  $y_1$ ,  $y_2$ , and  $P_t$ , in order to establish a direct connection with experimentally measured quantities. Study of the dominant subprocess cross-sections in lowest order  $2 \rightarrow 2$  QCD has shown that their angular dependences are similar enough to permit the approximate representation of the differential cross-section as

$$\frac{d^3\sigma}{dE_t d\eta_1 d\eta_2} = F(x_a)F(x_b)\sigma_{\text{eff}}(ab \rightarrow 12) \quad (1)$$

where  $x_a$  and  $x_b$  are the momentum fractions of partons  $a$  and  $b$ , respectively. In this approximation, one can extract the "Effective Structure Function" of the nucleon, where  $F(x) = G(x) + 4/9 [Q(x) + \bar{Q}(x)]$ , from a study of the differential cross section. ( $G(x)$  is the gluon component of the structure function;  $Q(x)$  and  $\bar{Q}(x)$  represent appropriate sums over its quark and antiquark components.) This is the "Single Effective Subprocess" approximation of Combridge and Maxwell <sup>1)</sup>.

Figure 1 shows the expected behavior of the differential cross section for one value of  $E_t$ , with one jet fixed at an  $\eta_1$  of zero. The fall-off with increasing  $\eta_2$  is caused by the rapid decrease in the structure

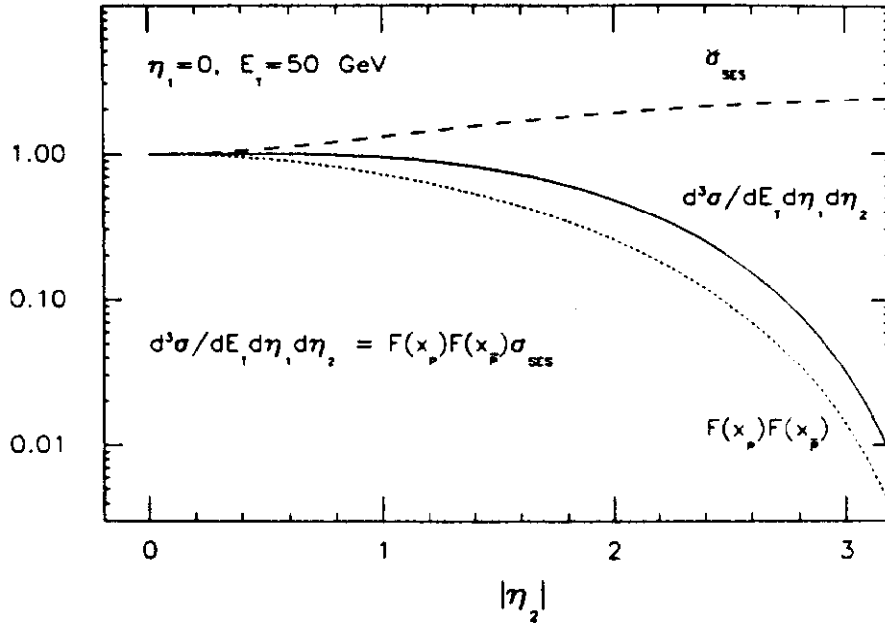


Figure 1: Expected behavior of the two-jet differential cross section in the Single Effective Subprocess approximation. (Note that here  $\sigma_{SES} = \sigma_{eff}$  of equation 1).

function  $F(x)$ , since  $x_a \cong \frac{E_t}{\sqrt{s}} e^{\eta_2}$ . At higher values of  $E_t$ , the cross section will lie on a similar curve, everywhere below the displayed curve. The structure function fall-off dominates the increase in  $\sigma_{eff}$  from the  $t$ -channel scattering amplitude pole.

The current study is based on  $24.5 \text{ nb}^{-1}$  of jet data collected in 1987. The experiment was triggered on the sum of uncorrected tower  $E_t$ , with thresholds that varied from 20 GeV to 45 GeV. (Most of the data was taken with thresholds of either 30 GeV or 45 GeV.) Jets were defined by a cone clustering algorithm, with a cone radius ( $\sqrt{\Delta\phi^2 + \Delta\eta^2}$ ) of 1.0. One jet was required to be central (cone centroid of  $|\eta_1| \leq 0.6$ ) and sufficient to trigger the experiment with 98% efficiency or greater. This requirement imposed a trigger hardening cut of 45 GeV to 75 GeV, depending on the trigger threshold. The second jet was allowed to fall anywhere in the fiducial region  $|\eta_2| \leq 2.8$ . The final data sample consisted of 5291 events.

As described elsewhere at this Workshop, we correct the raw jet energies using a relationship determined from the ISAJET event generator<sup>2)</sup> and an event simulation<sup>3)</sup>. The ratio of corrected to uncorrected jet  $E_t$  ranged from  $1.25 \pm .11$  for  $E_t = 45 \text{ GeV}$  to  $1.15 \pm .06$  for  $E_t = 225 \text{ GeV}$  (errors systematic). Resolution functions in  $E_t$  and  $\eta_2$  were established by studying the  $E_t$  imbalance in events

**CDF PRELIMINARY**

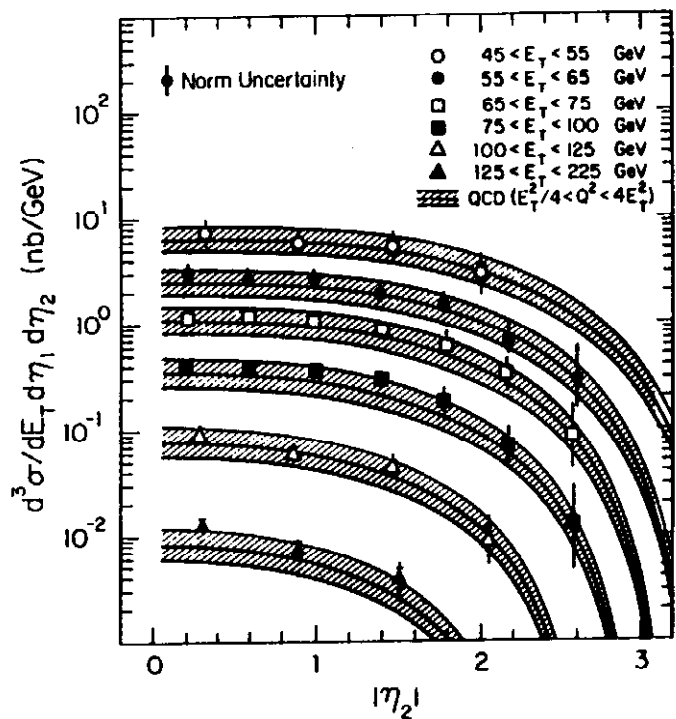


Figure 2: The two jet differential cross-section for  $|\eta_1| \leq 0.6$ , compared to a range of QCD predictions. Statistical and systematic errors (except overall normalization, shown separately) are indicated by inner and outer error bars.

**CDF PRELIMINARY**

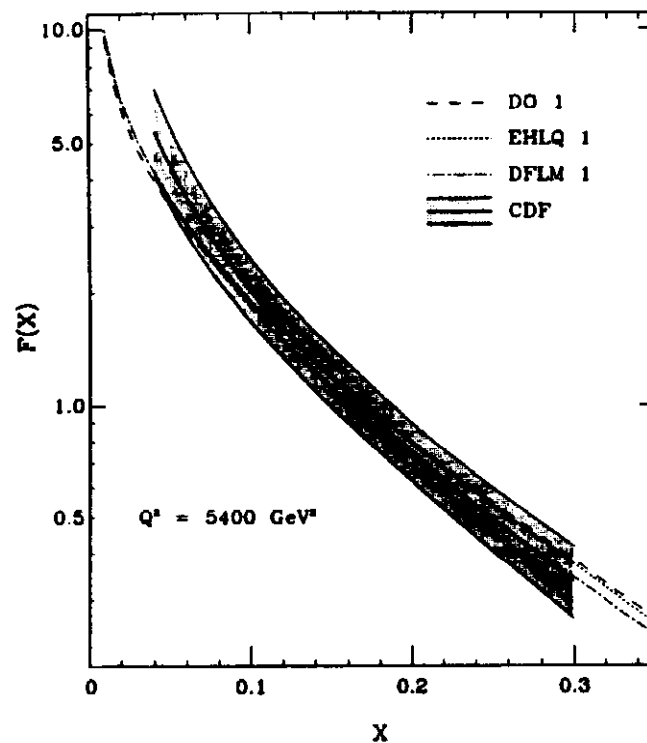


Figure 3: Proton effective structure function  $F(x)$ , compared to QCD evolution predictions. Shading indicates CDF systematic uncertainty.

with two leading jets in the region  $|\eta| \leq 0.6$ . The imbalances along the bisector of the two jets and the axis perpendicular to it are directly related to the resolutions in  $E_t$  and  $\eta_2$ , including the effects of gluon bremsstrahlung. The  $E_t$  resolution function is approximately Gaussian with  $\sigma = 11$  GeV for 50 GeV jets; the  $\eta_2$  resolution is better modeled by a Lorentzian with  $\Gamma = 0.25$  GeV (50 GeV jets).

We bin the data in  $E_t$  and  $\eta_2$  and deconvolve the measured cross-section to account for the above resolution effects. To do this, well-parametrized trial spectra in  $E_t$  and  $\eta_2$  are varied until a good fit to the measured distribution is obtained. The final  $\chi^2$  was 40 for 33 degrees of freedom. Figure 2 shows the measured two jet differential cross section for  $|\eta_1| \leq 0.6$  versus  $|\eta_2|$ , for 6  $E_t$  bins; a range of QCD predictions found by varying the  $q^2$  scale for  $E_t^2/4$  to  $4E_t^2$  is superimposed on the data. The QCD prediction shown uses EHLQ 2 structure functions<sup>4)</sup>. We have also tested DO, MRS, and DFLM structure functions<sup>5)</sup>. The MRS 2 structure functions are excluded by our comparison, which is dominated by experimental systematics. The leading systematic error is the uncertainty on the jet  $E_t$  measurement and correction, typical for this class of experiments.

As discussed above, the similarity of subprocess cross-sections enables us to extract an effective structure function  $F(x)$  for the nucleon from analysis of the differential cross-section. Our result for  $F(x)$  is displayed in figure 3. The CDF result is consistent with results from deep inelastic scattering within its systematic uncertainties.

### Three Jet Energy Sharing Variables -- 1988/89 Data

In addition to two-jet final states, QCD allows either incoming or outgoing partons to undergo bremsstrahlung of additional partons. If the bremsstrahlung event is hard and at a large angle, the additional radiated partons will become visible as separate jets in the final state. The simplest such events have only one hard bremsstrahlung and three jets. It is relatively improbable to have two such hard bremsstrahlungs in one event, therefore events with three or more clusters may be used for three-jet analysis with additional clusters contributing via resolution effects as in the previous section. Three jet events are characterized by the kinematic variables  $M_{3j}$ ,  $x_3$ ,  $x_4$ ,  $\cos\theta^*$ ,  $\psi^*$ , and  $\phi^*$ . Here  $M_{3j}$  is the invariant mass of the three-jet system, and  $x_3$  and  $x_4$  are defined as  $x_i = \frac{2E_i}{M_{3j}}$ .  $\theta^*$  is the angle between the incoming partons and the leading outgoing parton, and  $\psi^*$  is the angle between the plane described by the three final state partons and the plane described by the incoming and leading outgoing partons.  $\phi^*$  is the azimuthal angle of the leading outgoing parton and usually has no dynamical significance. Note that we use the convention<sup>6)</sup> that partons 1 and 2 are incoming, and partons 3-5 are outgoing, ranked by

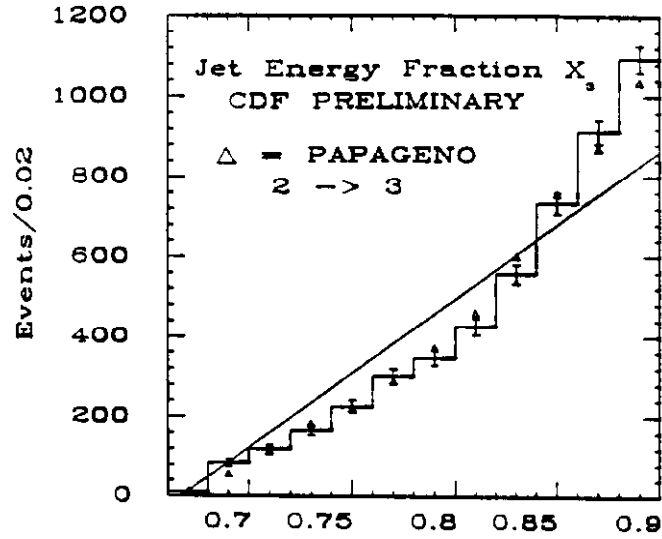


Figure 4: Three-jet energy fraction  $x_3$  compared to QCD (triangles) and phase space (solid line) predictions.

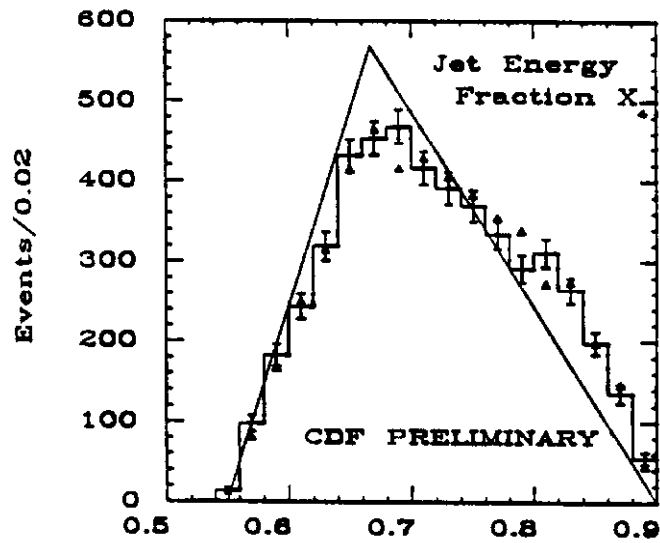


Figure 5: Three-jet energy fraction  $x_4$  compared to QCD (triangles) and phase space (solid line) predictions.

energy in the 3-jet CM frame. These variables describe the natural phase-space element for a three-jet system, so the method of analysis used is to search for deviations from uniform population density that are predicted by a QCD matrix element. In what follows we will focus on the energy sharing variables  $x_3$  and  $x_4$ . Previous studies<sup>7)</sup> of these distributions at the SP $\bar{P}$ S have been of limited statistical power for the question of resolving deviations from phase space distributions.

The current study is based on a sample of about  $2 \text{ pb}^{-1}$  of data collected in the 1988-89 run of CDF. This is less than 1/2 of the total data set. Analysis of the remaining data is in progress. All the events selected satisfied a total uncorrected  $E_T$  trigger with a threshold of 120 GeV. Events were then selected that had at least three jet clusters (cone radius of 0.7) each above 10 GeV in uncorrected  $E_T$ . We then correct the jet energy as described above, boost the  $\sim 89000$  events selected to the three-jet CM frame, and proceed with a second set of cuts in that frame. The cuts are:

$$\begin{aligned} M_{3j} &\geq 200 \text{ GeV}/c^2 \\ x_3 &\leq 0.9 \\ |\cos\theta^*| &\leq 0.72, 30^\circ \leq \psi^* \leq 150^\circ \end{aligned}$$

The mass cut constitutes an effective trigger-hardening requirement, and the second requires a third jet energetic enough to pass our  $E_T$  cut and be free of clustering bias. The angular cuts guarantee that all the jets used will have centroids in the fiducial region of  $|\eta| \leq 3.5$ .

After all cuts, we are left with a sample of 4973 events. Figures 4 and 5 show the projections of the Dalitz plot of  $x_3$  and  $x_4$  along the  $x_3$  and  $x_4$  axes. Also shown are phase-space predictions, and the expected distribution from a QCD  $2 \rightarrow 3$  parton level computation using the program PAPAGENO<sup>8)</sup> and EHLQ 1 structure functions<sup>4)</sup>. The data show the effect of the QCD matrix element rather clearly, especially in the increase in events at high  $x_3$ , suggesting a bremsstrahlung origin of the third jet (parton 5 in our notation).

## JET FRAGMENTATION STUDIES

### Fragmentation Function $D(Z)$ -- 1987 Data

The fragmentation of final-state partons into hadrons involves a non-perturbative component related to the final confinement of partons via hadronization. Nevertheless, at collider energies, perturbative QCD is expected to be the dominant mechanism of fragmentation when  $Z = P_{\text{had}}/P_{\text{jet}}$  is not close to unity and for final multiplicities of at least several particles. (In this section we use the scaling variable

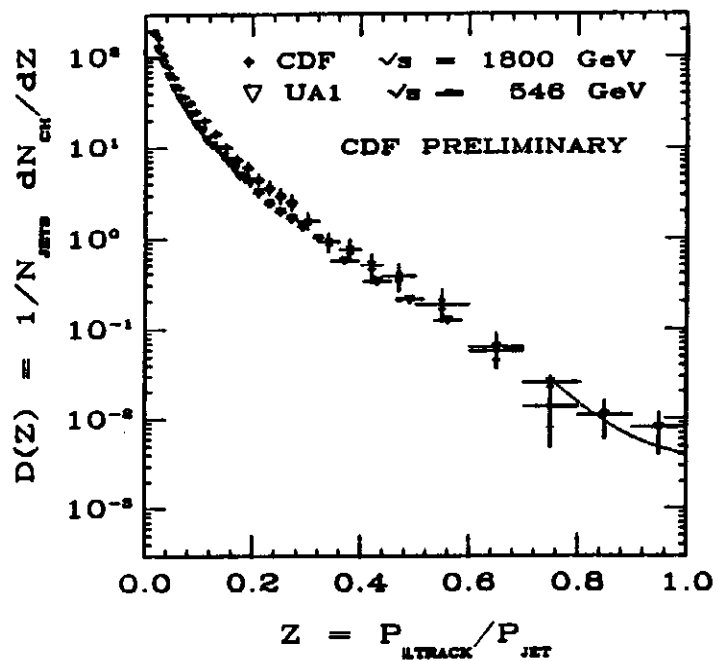


Figure 6: Charged fragmentation function  $D(Z)$ . CDF data show statistical and systematic errors. The dotted line represents a  $1\sigma$  limit to  $D(Z)$  for  $Z \geq 0.8$ , where background is appreciable. UA1 data are from ref. 9.

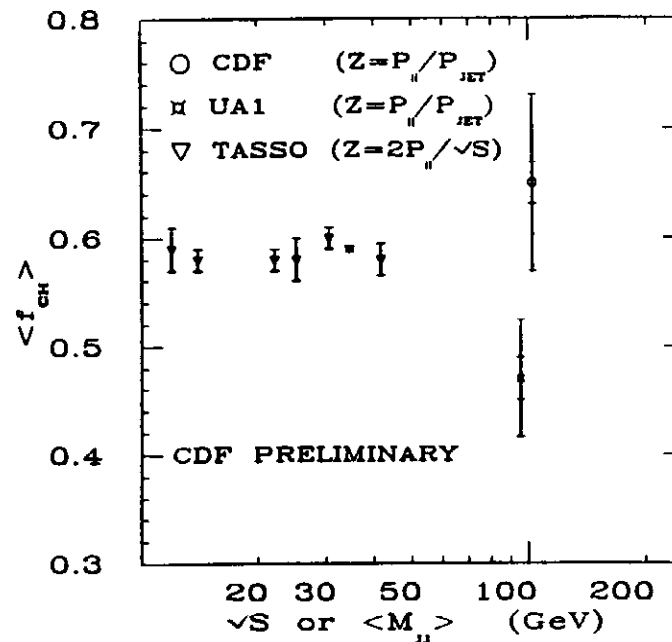


Figure 7: Charged momentum fraction as a function of  $Z$ , compared to data of refs. 9 and 11.

$Z$  defined as  $P_{\text{had}}/P_{\text{jet}}$  instead of  $P_{\text{had}}/E_{\text{jet}}$ , in order to maintain a convention established by previous collider measurements<sup>9)</sup>; the choice is somewhat arbitrary). In particular, perturbative QCD predicts<sup>10)</sup> characteristic deviations from scaling of the charged fragmentation function  $D(Z) = (1/N_{\text{jets}}) dN_{\text{charged}}/dZ$ , as a function of the  $q^2$  of the interaction.

For this analysis we used  $26 \text{ nb}^{-1}$  of 1987 jet data. The jet-finding algorithm and corrections were as described for the differential cross-section analysis. Jet momentum was computed using the vector sum of calorimeter tower energies. We required two jets above the hardware trigger threshold in the range  $|\eta| \leq 0.8$ , and nearly back-to-back in azimuth ( $180 \pm 30^\circ$ ). Other jet activity in the event was restricted to have less than  $\sim 20 \text{ GeV}$  of  $E_T$ . Final track-association cuts are done in the longitudinally boosted Lorentz frame of the di-jet system; to control systematics in this frame we limit the boost rapidity of accepted events to 0.6. Finally, only jets with  $|\eta| \leq 0.7$  are used in the fragmentation analysis. This combination of cuts yields 5541 events and 8609 jets.

Tracks passing cuts on their  $r$ - $\phi$  impact parameter, distance  $\Delta z$  from the interaction vertex, and hit quality, were associated with a jet if they were produced within a cone of  $48^\circ$  about the axis of the jet ( $\eta$  to the jet axis of 0.8 or greater), and if they had a momentum parallel to the axis  $P_{\parallel} \geq 0.6 \text{ GeV}/c$ . This momentum cut insures that all tracks in our boost range have  $P_t$  (to the beam axis) of 400 MeV/c or greater, where the CTC is fully efficient.

Track finding efficiency was estimated by merging simulated tracks into data and by Monte Carlo simulation. We restrict the study to dijet mass  $M_{jj} \leq 200 \text{ GeV}/c^2$ , where we find the tracking efficiency to be high ( $\sim 90\%$ ). The raw  $D(Z)$  is corrected for this efficiency, for geometrical acceptance effects, and for an estimated underlying event contribution. We must also unfold the effects of the falling spectra in jet  $E_T$ , and for the effects of smearing feed-down due to the falling of  $D(Z)$  itself.

Figure 6 shows our result for the charged fragmentation function  $D(Z)$ . The function lies somewhat higher than the UA1 result over much of its range, and falls more steeply. This also seen in the integrated charged fraction

$$\langle f_{\text{ch}} \rangle = \int_0^1 Z D(Z) dZ \quad (2)$$

displayed in figure 7 for various experiments. In the region below  $Z$  of 0.02 our cut on  $P_{\parallel}$  means that we must extrapolate  $D(Z)$  from a fitted functional form. This is expected to be a 2-5% effect on the integral.

Our result is  $\langle f_{ch} \rangle = 0.65 \pm 0.08$  (sys.), where the dominant source of error is the knowledge of the jet energy scale.

In figure 8 we show  $D(Z)$  vs.  $s$  for TASSO data<sup>(11)</sup> and a preliminary CDF result vs.  $M_{jj}^2$ . Both sets of data show the same trend, an increased peaking at low  $Z$  as  $q^2$  increases. We have displayed a separate error bar showing the overall normalization uncertainty for each band. The fitted curves are of the QCD-motivated form<sup>(10)</sup>  $\gamma + \delta \ln(M_{jj}^2)$ . The data is consistent with the evolution expected from collinear gluon emission.

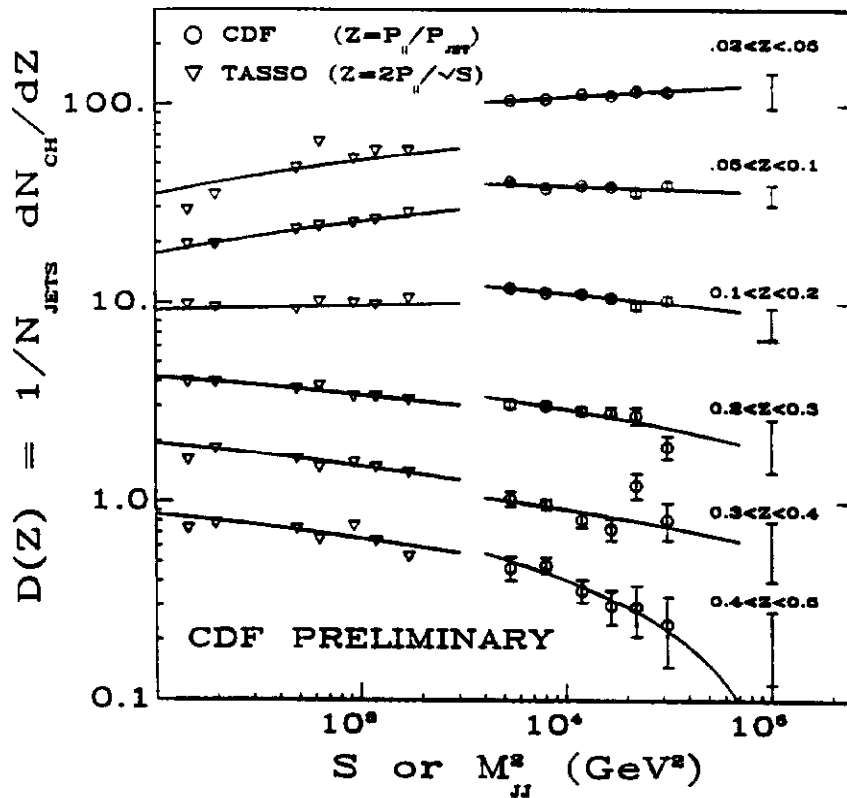


Figure 8: Evolution of the charged fragmentation function  $D(Z)$  vs.  $M_{jj}$  (CDF) or  $s$  (TASSO [11]) for six intervals in  $Z$ .

## D\* Production in Jets -- 1987 Data

The most exclusive of the processes considered in this paper will be the production of heavy quarks inside jets. This process is calculable in perturbative QCD, with the non-perturbative contribution expected to be very small<sup>(12, 13)</sup>. One specific prediction that can be tested is the expected rate of  $D^*$

production per identified jet. We present here a measurement of the  $D^*$  production rate for fractional momentum  $Z \geq 0.1$  where  $N(D^{*\pm}) = N(D^{*+}) + N(D^{*-})$ . The main mechanism expected for this process is the splitting of gluon jets into  $c\bar{c}$  and  $b\bar{b}$  pairs<sup>12)</sup>. Since, in relevant ranges of kinematical parameters, jets at CDF are preponderantly ( $\sim 75\%$ ) gluon-initiated<sup>14)</sup>, this higher-order process becomes competitive and indeed dominant over direct heavy-quark production.

The basis of the  $D^*$  search is the detection of the combination  $K^-\pi^+\pi^+$  coming from the decay of the  $D^{*+}$  into  $D^0\pi^+$ , and the subsequent decay  $D^0 \rightarrow K^-\pi^+$  (as well as the charge conjugate mode for  $D^{*-}$ ). Because the value  $\Delta_M = M_{K\pi\pi} - M_{K\pi}$  is only  $145 \text{ MeV}/c^2$ , the CDF central tracking chamber (CTC) has very good resolution in  $\Delta_M$  ( $\sim 0.6 \text{ MeV}/c^2$ ) once the slow pion is above a threshold  $P_t$  of  $300 \text{ MeV}$ . Our understanding of the resolution is limited by the systematics of drifting electrons at large cell-crossing angles in the CTC.

Jet-finding, and jet energy corrections are as described under the measurement of the differential cross-section, for a luminosity of  $\sim 21 \text{ nb}^{-1}$ . After requiring jets to have corrected  $E_t$  of  $30 \text{ GeV}$  or greater, one is left with a data sample of  $\sim 32000$  jets with  $\langle E_t \rangle = 46.6 \text{ GeV}$ . Charged particle tracks were reconstructed in the CTC and constrained to the event vertex. Tracks were required to have  $P_t > 300 \text{ MeV}/c$ ,  $|\eta| \leq 1.2$ , and to pass loose track-quality cuts. We then formed  $K\pi$  and  $K\pi\pi$  mass combinations, using  $K$  and  $\pi$  assignments for all tracks. To associate a  $K\pi\pi$  combination with a jet, its rapidity with respect to the jet axis had to be positive. In ambiguous cases, the most positive was chosen. In addition, assuming the  $D^*$  mass for the combination, we required the fractional momentum  $Z$  of the  $D^*$  to be greater than  $0.1$ . This kinematic cut allows direct comparison with other collider measurements<sup>15)</sup>.

To further improve the signal-to-noise ratio, we chose only combinations with  $|M_{K\pi} - M_{D^0}| \leq 3\delta$ , where the quantity  $\delta$  was computed by propagating the track parameter uncertainties on an event-by-event basis ( $\langle \delta \rangle = 19 \text{ MeV}$ ). We also cut on the kaon polar angle  $\theta^*$  in the  $D^0$  rest frame --  $|\cos\theta^*| \leq 0.8$ . This reduces the background from spurious combinations peaked along the jet axis. With these cuts, we estimate from Monte Carlo (simulated  $D^*$ 's merged with real jets) that the overall reconstruction efficiency for produced  $D^*$ 's with  $Z \geq 0.1$ , and with observed  $\Delta M$  between  $144.5$  and  $146.5 \text{ MeV}/c^2$ , is  $37\% \pm 9\%$ , of which  $\sim 64\%$  is from tracking. The uncertainty is dominated by our limited knowledge of the multiplicity of  $D^*$ -containing events and of the mass resolution.

The above analysis yields the results shown in figure 9. There is a clear excess of events in the bin centered at  $145.3 \text{ MeV}/c^2$ . As may be seen in the inset to figure 9, a control sample of "wrong-sign" (e.g.

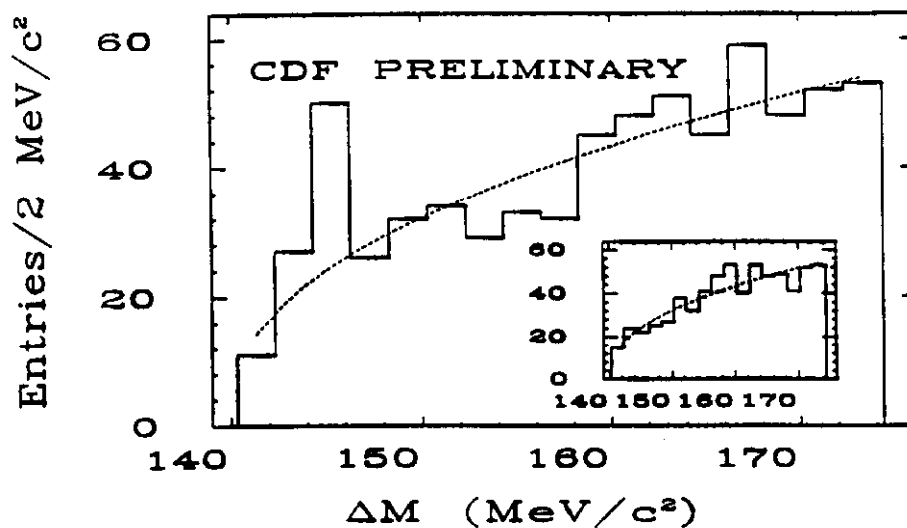


Figure 9: Mass difference  $\Delta M = M_{K_{\text{SK}}\pi} - M_{K_S\pi}$  after all cuts. The inset shows the same distribution for wrong-sign mass combinations.

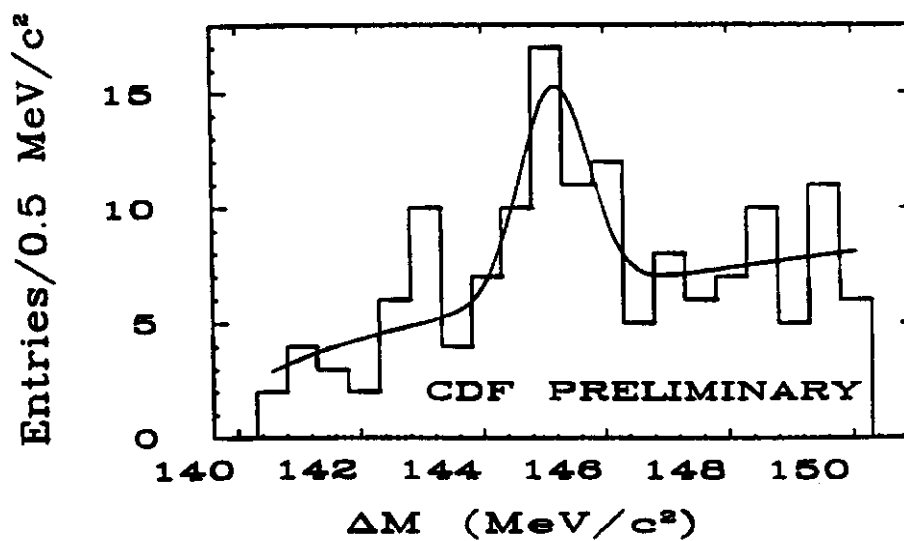


Figure 10: Mass difference  $\Delta M$  on expanded scale, showing fits to background and signal.

$K^+\pi^+\pi^-$  and charge conjugate) shows a smooth background without apparent signal. We fit the two distributions simultaneously to a background function of the form  $a(\Delta M - m_{\pi})^b$  and, in the case of the "right-sign" combinations, a Gaussian for the signal contribution. This fitting procedure results in an estimate of the signal of  $25 \pm 8 \pm 2 D^*$  's in our sample, where the first error is statistical, and the second represents the systematic uncertainty on the background subtraction. Figure 10 shows the results of the fitting procedure on an expanded scale.

Using a Monte Carlo, we estimate the effects of smearing due to the  $E_t$  and  $Z$  spectra of our jets. This leads to an expectation of  $1.1 \pm 0.2 D^*$  's ( $Z \geq 0.1$ ) produced for each such  $D^*$  observed. Together with the reconstruction efficiency quoted above and the branching ratios for this decay mode<sup>16)</sup>, we obtain:

$$N(D^{*\pm})/N(\text{jet}) = 0.10 \pm 0.03(\text{stat.}) \pm 0.03(\text{sys.}) \quad (\text{for } Z \geq 0.1)$$

This result is consistent with the QCD estimates of ref. 12, and with previous measurements<sup>15)</sup>.

## SUMMARY

We have presented preliminary results from a variety of QCD-generated jet processes. The differential cross-section shows the behavior expected from lowest order QCD  $2 \rightarrow 2$  scattering. The charged fragmentation function  $D(Z)$  shows evidence of evolution in  $q^2$ . Three-jet phase space variables  $x_3$  and  $x_4$  show clearly the need for a non-constant matrix element, such as provided by perturbative QCD. The production of charged  $D^*$  in jets, as well, shows agreement with the perturbative mechanism. One may conclude that perturbative QCD provides a powerful tool for the understanding of hadronic jet behavior at the highest collision energies currently available.

## APPENDIX - -THE CDF COLLABORATION

ANL - Brandeis - University of Chicago - Fermilab - INFN, Frascati - Harvard - University of Illinois - KEK - LBL - University of Pennsylvania - INFN, University and Scuola Normale Superiore of Pisa, Purdue - Rockefeller - Rutgers - Texas A&M - Tsukuba - Tufts - University of Wisconsin.

## REFERENCES

- 1) B. Combridge and C. Maxwell, Nucl. Phys. B239, 429 (1984).

- 2) F. Paige and S. Protopopescu, in *Proceedings of the Summer Study on the Physics of the Superconducting Supercollider, Snowmass, CO, 1986*, R. Donaldson and J. Marx, edit., pp. 320-326.
- 3) S. Kuhlmann, Ph.D. thesis, Purdue University, 1988 (unpublished).
- 4) E. Eichten, I. Hinchliffe, K. Lane, and C. Quigg, *Rev. Mod. Phys.* **56**, 579 (1984).
- 5) D. W. Duke, and J. F. Owens, *Phys. Rev.* **D30**, 49 (1984);  
A. D. Martin, R. G. Roberts, and W. J. Sterling, *Phys. Rev.* **D37**, 1161 (1988);  
M. Diemoz, F. Ferroni, E. Longo, G. Martinelli, *Z. Phys.* **C39**, 21 (1988).
- 6) F. A. Berends *et al.*, *Phys. Lett.* **103B**, 124 (1981).
- 7) G. Arnison *et al.*, *Phys. Lett.* **158B**, 494 (1985).
- 8) I. Hinchliffe, personal communication.
- 9) G. Arnison *et al.*, *Nucl. Phys.* **B276**, 253 (1986).
- 10) G. Altarelli, *Phys. Rep.* **81**, 1 (1982).
- 11) M. Althoff *et al.*, *Z. Phys.* **C22**, 307 (1984).
- 12) V. Barger and R. J. N. Phillips, *Phys. Rev.* **D31**, 215 (1985);  
G. Köpp, J. H. Kühn, and P. M. Zerwas, *Phys. Lett.* **153B**, 315 (1985);  
F. Halzen and P. Hoyer, *Phys. Lett.* **154B**, 324 (1985);  
A. Ali and G. Ingelman, *Phys. Lett.* **156B**, 111 (1985).
- 13) A. H. Mueller and P. Nason, *Nucl. Phys.* **B266**, 265 (1986).
- 14) J. F. Owens, E. Reya, and M. Glück, *Phys. Rev.* **D18**, 1501 (1978).
- 15) G. Arnison *et al.*, *Phys. Lett.* **147B**, 222 (1984);  
M. Della Negra, *Proceedings of the 6<sup>th</sup> Topical Workshop on Proton-Antiproton Collider Physics, Aachen, 1986*, K. Eggert, H. Faissner, and E. Radermacher, edit., pp. 181-212.
- 16) J. Adler *et al.*, *Phys. Lett.* **B208**, 152 (1988);  
J. Adler *et al.*, *Phys. Rev. Lett.* **60**, 89 (1988).